Design of compressed variable stiffness panels with steering-thickness coupling

Machado, Tulio Gomes de Paula; Hernandes, José Antonio; Capacia, Victor Nicoláo; Castro, Saullo Giovani Pereira

DOI
10.2514/6.2021-0568

Publication date
2021

Document Version
Final published version

Published in
AIAA Scitech 2021 Forum

AIAA SciTech Forum
11–15 & 19–21 January 2021, VIRTUAL EVENT
AIAA Scitech 2021 Forum

10.2514/6.2021-0568

Design of compressed variable stiffness panels with steering-thickness coupling

Tulio Gomes de Paula Machado* and José Antonio Hernandes†
Department of Aeronautical Engineering, ITA – Technological Institute of Aeronautics, 12228-900 São José dos Campos, SP, Brazil

Victor Nicoláo Capacia ‡
Department of Mechatronics and Mechanical Systems, University of São Paulo Polytechnic School, 05508-010, São Paulo, SP, Brazil
EMBRAER, 12227-901, São José dos Campos, SP, Brazil

Saullo Giovani Pereira Castro§
Faculty of Aerospace Engineering, Delft University of Technology, 2629 HS Delft, Netherlands

I. Nomenclature

a	=	Length
b	=	Width
d	=	Characteristic distance
f	=	Fitness
F	=	Force
g_i	=	Penalty factor functions
h	=	Height
m_{unit}	=	Mass of the unit cell
N_{stf}	=	Number of longitudinal stiffeners
r_s	=	Steering radius
t	=	Thickness
T_0, T_1	=	Interpolation angles at two reference points for linear variations
T_{mn}	=	Lagrangian interpolation angle at the reference point
θ	=	Fiber steering angle
κ	=	Tow path curvature
λ	=	Buckling load factor
ϕ	=	Rotation angle between systems of reference
$\bar{\mathbf{x}}$	=	Design variable vector

Automated manufacturing techniques of composite materials such as automated fiber placement (AFP) and continuous tow shearing (CTS) can be configured to produce fibers that follow curvilinear paths, resulting in variable laminate properties that can be tailored to a large range of engineering applications. The present study focuses on the design and optimization of a wing upper skin exploring the coupled thickness build-up that is inherent to the CTS process and appears in the AFP process when continuous tows are used with an overlapping design approach. The steering-thickness coupling comes from constant-volume requirements and is an extra nonlinear constraint that poses additional challenges to the design and optimization, rendering conventional two-step approaches based on lamination parameters and total thickness ineffective. The number of longitudinal stiffeners, cross-section shape and laminate configuration are treated as design variables in a single-step optimization driven by a classical

*Corresponding author, MSc Graduate, email: tuliomachado10@gmail.com
†Professor at Department of Aeronautical Engineering, ITA
‡Structures Engineer, EMBRAER, PhD Student at University of São Paulo Polytechnic School
§Corresponding author, Assistant Professor in the Department of Aerospace Structures and Materials, email: S.G.P.Castro@tudelft.nl

genetic algorithm. Knowing the current state of angle distributions proved to be important while calculating the coupled thickness build-up. The optimization problem is constrained by the critical linear buckling load, herein calculated using finite elements with MSC Nastran®, and by manufacturing and design constraints, such as the minimum steering radius of AFP and CTS and common design guidelines for laminated composites. The results are compared with an optimized baseline design using conventional straight-fibre laminates to quantify how the design is changed in terms of overall geometry, buckling loads and structural weight.

II. Introduction

The emergence of novel automated manufacturing techniques in recent years allowed the creation of continuously varying fiber laminates, referred as Variable Stiffness Laminates (VSL). Automated Fiber Placement (AFP) and Continuous Tow Shearing (CTS) [1] are examples of automated manufacturing processes that can steer fibers within the plane, by depositing fibers following a curvilinear path within the laminate plane. Fiber steering creates spatially variable mechanical properties within the laminate plane, enhancing tailoring capabilities of VSL due to more efficient in-plane load paths, resulting in weight savings that can not be achieved using traditional laminates [2]. Substantial improvements in buckling loads were achieved by varying the laminate stiffness in the direction perpendicular to the applied load due to a redistribution of the primary loads from the center section of the panel to the simply supported sides of the panel [2, 3].

Regarding AFP and CTS processes, the manufacturing of continuously varying fiber laminates are limited by the minimum fiber steering radius that the machine is capable of performing without compromising laminate quality. Due to the different machine operation and physical phenomena involved in both process, AFP and CTS have different limitations regarding the minimum fiber steering radius. Additionally, both processes produce variations in laminate thickness that are coupled to the fiber steering angle [4].

Genetic algorithms (GA) as an optimization tool have been widely employed to solve engineering problems and are capable of searching for the best solution in non-convex design spaces better than well established gradient-based methods, as the seek for optimal solution is performed through random probability methods [5]. Applications of GA in the optimization of composites designs include laminate stacking sequence of several plates under buckling and strength constraints [6] and stiffened panels [7] and wingbox structures. For the latter, McIhagga et al. [8] compared different search schemes against GA. Wan et al. [9] performed aeroelastic tailoring to minimize the winbox skin weight, using the ply-thicknesses as design variables. Arizono et al. [10] used a GA to find the minimum weight of a supersonic wing structure constraining the static strength, local buckling, and minimum flutter speed. Gasbarri et al. [11] performed aeroelastic tailoring of a composite wing using sequential quadratic programming to find the maximum flutter velocity, while employing a GA to search for optimum composite layups, avoiding local optima. Castro et al. investigated: fast GA schemes with progressive mesh refinement to allow for more exploration of the design space [12]; the effect of GA parameters [13]; comparisong with gradient-based methods [14]; and different parameterization schemes [15]. Jin et al. [16] used parallel GA for large wingbox optimizations. More recently, Liguori et al. [17] applied GA in the optimization of a variable-angle tow wingbox construction considering post-buckling constraints.

In multi-step or hybrid optimization schemes, in a first step gradient-based methods are used to find the optimal lamination parameters and thickness, whereas GA is employed in a second step as a tool to retrieve the actual fiber orientations [18–21]. However, when the thickness depend on the final fiber orientations, as in the present study with steering-thickness coupling, the laminate stiffness cannot be optimized in a separate step because the outcome of the orientation-retrieving process would modify the thickness variable that was assumed to be an independent variable in the first step.

The present work focuses on the design parameterization and optimization of a wing upper panel constructed with variable stiffness laminates allowing steering-thickness coupling. Using a classical genetic algorithm, the panel geometry, fiber path and laminate stacking sequence are optimized in a single step to minimize the structural weight. The single-step optimization approach allows a straightforward description of the actual fiber orientations and steering angles, whereby the coupled thickness variation can be calculated based on constant volume requirements [4, 22]. By employing a Lagrangian interpolation scheme and treating the reference fiber orientation angles as design variables, the variable thickness coupling is simplified once the steering angle is directly obtained.

Loading conditions in the upper skin are derived from a real aircraft up-bending load case. Ideally, a fast tool for the buckling assessment should be used due to the vast number of evaluations expected by the GA-based optimizer. Bisagni and Vescovini [23] presented a fast tool that can be used during the preliminary design of isotropic and composite panels

subject to axial compression, whereby GA is used in the optimizations. Vescovini and Bisagni [24, 25] also demonstrate a fast semi-analytical buckling model for the buckling of constant-stiffness composite panels with omega stiffeners. For variable-stiffness plates, Vertonghen and Castro [22] presented a suitable semi-analytical formulation for the purposes of the present study, which, however, cannot be used due to the stiffening plate elements, unless some strategy of connecting multiple domains is implemented, such as penalizing the strain energy [25–27]. Given the complications aforementioned complications with implementing a semi-analytical model, the linear buckling analyses are herein performed by means of finite elements with MSC Nastran®. A design parameterized using straight-fiber laminates is optimized using the same algorithm to serve as a baseline for comparison to the optimized variable stiffness designs. Both AFP and CTS techniques are explored by means of different constraining steering radius in the optimization. The overall laminate configuration, in terms of geometry, mass, layup and fiber variations are compared to the baseline design and among each other.

III. Variable Stiffness Laminates

The simplest manner to describe a curvilinear fiber path is to assume that the fiber orientation angle θ varies linearly in one direction between two reference points A and B, as originally proposed by [3]. This approach was later generalized to allow variation along any arbitrary axis x' by [28] as shown in Fig. (1a).

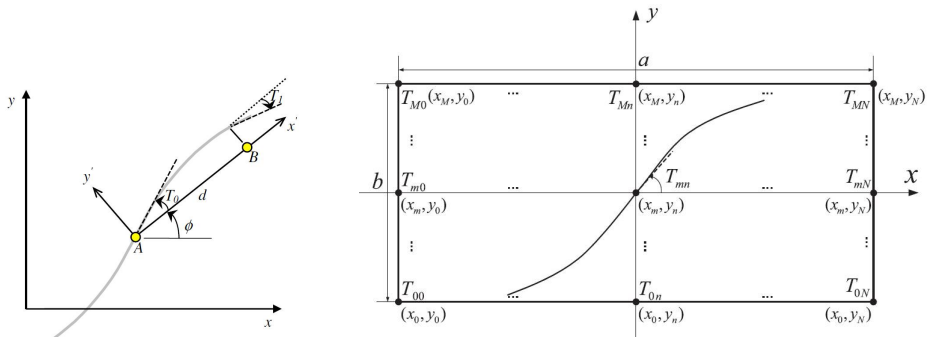

(a) Linear Variations of Steering Angle [29]

(b) Nonlinear variation of fiber orientation [18]

Fig. 1 Methods of Curvilinear Fiber Path Modeling

Equation (1) describes the fiber orientation angle with respect to the coordinate x', where T_0 and T_1 are, respectively, the prescribed fiber orientation angles at the reference points A and B, d is the characteristic distance between the reference points and ϕ is the rotation angle between the local coordinate system with respect to the global coordinate system. The reference path of steered tow over the plane can be obtained by the first derivative of the fiber path $dy'/dx' = \tan\theta(x')$.

$$\theta(x') = \phi + (T_1 - T_0)\,\frac{|x'|}{d} + T_0 \tag{1}$$

More complex fiber paths can be modeled using the Lagrange polynomial scheme proposed by [18, 30] for rectangular domains and by Capacia et al. [31, 32] using an arbitrary distribution of control points. Prescribed fiber angles T_{mn} at the $M{\times}N$ reference points placed over the plane, as shown in Fig. (1b), determine the polynomial coefficients of the fiber path. The main advantage of this scheme is that the coefficient of each term T_{mn} is already the fiber angle at the corresponding reference point (x_m, y_n). The Lagrange polynomial that describes the nonlinear variation of the steering angle is represented by Eq. (2), where (x_i, y_i), (x_m, y_m) are the coordinates of reference points in the plane.

$$\theta(x,y) = \sum_{m=1}^{M}\sum_{n=1}^{N} T_{mn} \prod_{\substack{i=1\\ i\neq m}}^{M}\left(\frac{x - x_i}{x_m - x_i}\right) \prod_{\substack{j=1\\ j\neq n}}^{N}\left(\frac{y - y_j}{y_n - y_j}\right) \tag{2}$$

Manufacturing limitations of variable stiffness laminates are related to the minimum steering radius the machine is capable of performing without inducing manufacturing defects in the laminate. The angular trajectory of the reference

fiber path is related to the Cartesian trajectory by:

$$\frac{dy}{dx} = \tan\theta(x, y)$$

such that the steering radius r_s is defined as the inverse of the tow path curvature κ, which is related to the trajectory of the tow path using Cartesian coordinates as:

$$r_s = \frac{1}{\kappa} = \frac{\left(1 + \left(\frac{dy}{dx}\right)^2\right)^{\frac{3}{2}}}{\left|\frac{d^2y}{dx^2}\right|} \tag{3}$$

A. Automated Fiber Placement (AFP)

Emerging in the late 1980s [20], the Automated Fiber Placement (AFP) creates curvilinear fiber paths by applying in-plane bending in the fiber tow as pre-impregnated steered fibers are laid down onto the mold surface [1]. For small steering radiusm manufacturing defects such as wrinkling, out-of-plane edge buckling, local folding [33] start to appear as a result of the in-plane bending, affecting laminate quality. Hence, a minimum allowed steering radius for AFP of 500 mm have been considered in this work [1, 33]. AFP requires several passes of the machine head to fully cover the entire laminate surface, whereby the head is shifted in a direction perpendicular to the angle variation after the machine completes a single pass. Formation of gaps and overlaps are observed between continuous shifted tows, as illustrated in Fig. 2a. Constant thickness layers can also be manufactured by means of tow cut-and-restart, as shown in Fig. 2b, with the drawback of increased manufacturing time due to the intermittent operation of the robots [2].

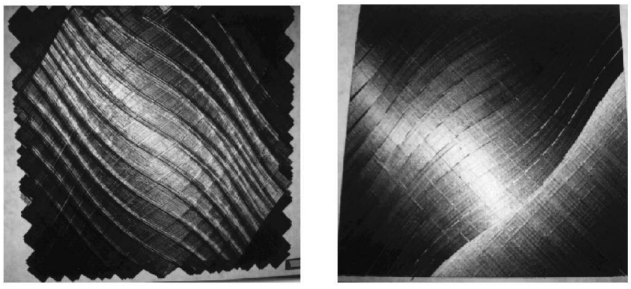

(a) Local thickening pattern (b) Constant thickness

Fig. 2 AFP Panels with (a) local thickening pattern and (b) constant thickness due to cut-restart technique [28]

By finding a shifting value that minimize the formation of gaps, Blom [2] defines the minimum effective tow width. The effective tow width w_e, illustrated in Fig. (3), is a function of the nominal tow width w_{tow} and the steering angle $\theta(x, y)$, as given by Eq. (4) [2]. Therefore, the minimum effective tow width corresponds to the minimum steering angle $\theta(x, y)$ along the steering direction represented by the x-axis in Fig. (3).

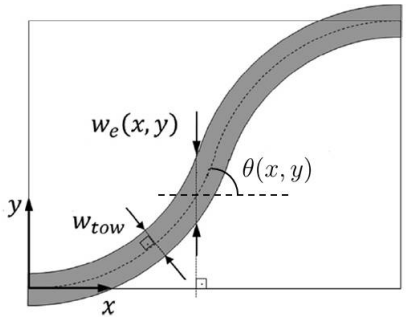

Fig. 3 Effective Tow Width Definition - adapted from [4]

$$w_e(x, y) \approx \frac{w_{tow}}{\cos(\theta(x, y))} \tag{4}$$

A smeared thickness distribution over the laminate is assumed, as demonstrated by [4] to be approximately described by Eq. (5) in terms of the minimum effective width. The main advantage of the smeared thickness approach regarding finite element modeling is that local thickening is simplified by a continuous thickness distribution over the plane, avoiding extremely refined meshes to model local thickening regions properly. The smeared thickness assumption for AFP panels has been compared with a discrete representation where all overlaps are modelled, leading to very close results [22, 34].

$$t_e(x, y) = t_{tow} \frac{w_e(x, y)}{w_{tow}} \approx \frac{t_{tow}}{\cos\theta(x, y)} \tag{5}$$

B. Continuous Tow Shearing

The continuous tow shearing (CTS) process steers dry or semi-dry fiber tows using in-plane shearing, guiding the tow along a desired path. A resin film is heated to impregnate the tows in-situ after shearing and deposition [1]. As a result, prototype testing has shown that the CTS can manufacture variable-stiffness laminates with the tows curved significantly more than AFP [1, 35], achieving a minimum steering radius of only 50 mm [1]. Despite being in its early stages of development, shifting in CTS technique allows fibers within the tow to follow an identical curve but simply shifted along the assigned shifting direction, achieving perfect tessellation [1], without producing gaps or overlaps commonly found in AFP designs. The major difference between CTS in comparison to AFP regarding the tow steering mechanism is shown in Fig. (4).

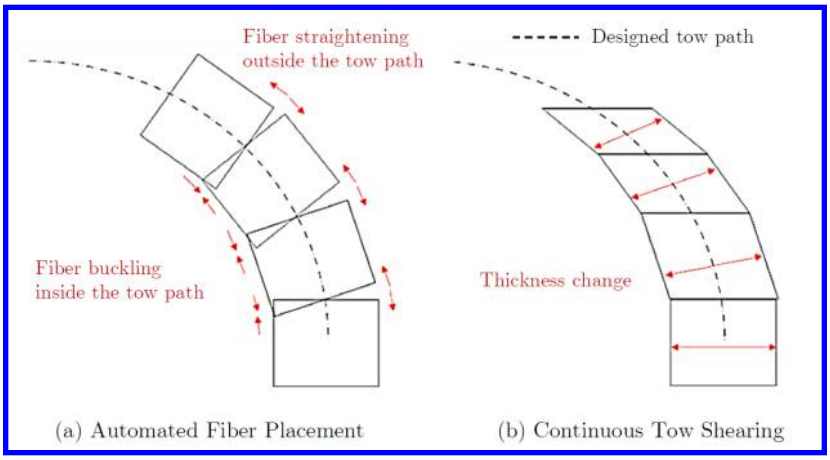

Fig. 4 Differences in Tow Steering from AFP and CTS - adapted from [1]

Thickness variations occur as in-plane shearing is applied to the tow in order to keep a constant volume. This is an inherent feature of laminae produced by means of CTS [35]. By assuming that the tow volume does not change during the shearing process. Castro et al. [4] showed a simple expression for the sheared tow t in terms of the steering angle θ and nominal tow thickness t_0, given in Eq. (6). Thickness variations in CTS panels are continuous due to the shear deformation which the tows are subjected, whereas thickness build-up of AFP process occurs due to overlapping regions.

$$t = \frac{t_0}{\cos\theta(x)} \tag{6}$$

IV. Finite Element Model

The finite element model is extracted from a double half-bay model representation, proposed in the work of Fenner [36], consisting of two halves of adjacent wing bays separated by the rib in the middle. The representative unit cell is a fraction of the entire panel, consisting of one longitudinal stiffener attached to the skin, whose width is equal to the spacing between adjacent stringers, that extends longitudinally from one adjacent mid-bay to the other as delimited by

the red box region shown in Fig. (5a). The unit cell cross-section geometry is represented in Fig. (5b) in terms of optimization design variables. Values assigned to the design variable b are integer fractions of the total width of the wing bay panel W - in this work, $W = 840$ mm. The unit cell approach is convenient during a preliminary design phase where only few design characteristics are completely defined and frequent design modifications require a rapid tool for concept validation.

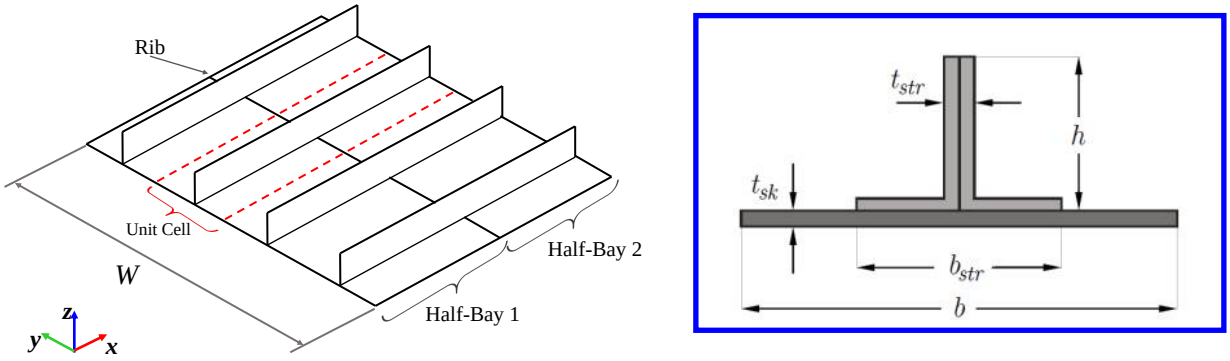

(a) Unit cell representation of a stiffened panel

(b) Cross-section of the stiffened panel unit cell

Fig. 5 Unit Cell Representative Section within Stiffened Panel Bay

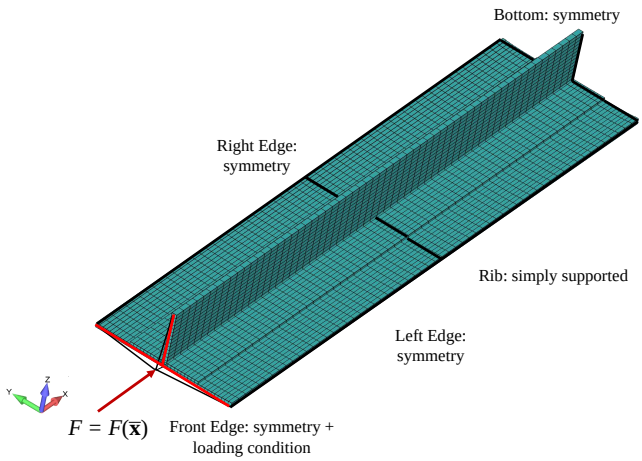

Fig. 6 Double Half Bay Symmetry Finite Element Modeling

The finite element model is derived from the unit cell representation using symmetry boundary conditions over a representative unit cell of the panel. Symmetry boundary conditions are depicted in Fig. (6). Displacement of lateral edges are constrained in y-direction and rotations with respect to x and z-axis. Unit cell front edge and bottom edge are constrained in rotation with respect to y and z-axis. Also, nodal displacements in x-axis of nodes at the bottom edge are constrained. The rib placed in the middle of the representative section unit cell supports displacements in the z-axis. The load is distributed in the front edge by means of a rigid element and nodal force $F(\bar{\mathbf{x}})$ applied to a master node. In the proposed optimization scheme, the acting force $F(\bar{\mathbf{x}})$ is a function of the design variables $\bar{\mathbf{x}}$, calculated consistently for each individual configuration of the stiffened panel unit cell based on geometry aspects of the unit cell such as stringer spacing, stringer height and thickness distribution.

In the optimization framework herein proposed, all design variables can be related to the representative unit cell, reducing the amount of optimization design variables and computational costs. For all cases under study, the stringer

is always manufactured with constant stiffness laminates, whereby two laminate properties are required: one for the stringer web; and another for the stringer foot. The longitudinal stringer is composed of a pair of L-shaped stringers joined in their shared mid-plane to form a T-shape stringer, which makes the laminate at the stringer web symmetric over the mid-plane. Thus, the stringer foot laminate can be asymmetric.

The properties for carbon-epoxy laminate used in this study are E_1 = 137.88 GPa, E_2 = 11.72 GPa, ν_{12} = 0.3, G_{12}= 4.825 GPa, ρ = 1600 kg/m^3 and t_{ply} = 0.1524 mm [37]. Note that the same material properties are assumed for the baseline straight-fiber structures, AFP- and CTS-manufactured structures, disregarding differences in material properties that will occur due to the different manufacturing processes.

A. Modeling of VSL

Every layer in the skin laminate that contains a curvilinear fiber is modeled after a Lagrangian polynomial interpolation at the T_{mn} reference points, defining fiber orientations on each element centroid. By using the smeared thickness formulation, a continuous distribution of thickness is assigned to the mesh, not modeling the local thickening regions of AFP laminates. Hence, the FE modeling is the same regardless of the manufacturing method (AFP or CTS). The variable thickness, per ply, as function of fiber orientation is modeled after the trigonometric relation between the nominal thickness t_{ply} and its spatial orientation $\theta(x, y)$, expressed by Eq. (7). The element thickness t_e is determined by the sum of the thicknesses of all plies stacked in the laminate of the element.

$$t^*_{ply}(x_i, y_i) = \frac{t_{ply}}{\cos\theta(x, y)} \approx \frac{t_{ply}}{\cos\theta(x_i, y_i)} \tag{7}$$

With the default setting, MSC Nastran® calculates the thickness of the plate element with respect to the reference plane determined by the nodes within the element [38], creating a symmetrical thickness distribution profile shown in the laminate cross section. However, this is not consistent to the manufacturing of these panels, as the steered fibers are placed over a flat mold surface. Therefore, an element offset is applied to every element in the skin mesh, in a distance of $t_e(x_i, y_i)/2$ along the positive z-axis of the element coordinate system, to account for thickness variations measured from the mold reference plane.

V. Optimization Framework

The genetic algorithm (GA) herein proposed was developed using Python programming language following a classic GA structure. Selection of the next population is performed based on the ranking of the current population according to the fitness evaluation. Genetic operators such as cross-over, mutation, and permutation are applied in this step to ensure genetic diversity to the next generation. Proportions and probabilities of the genetic operators were based on the work of [13], with elitism rate of 10%, probability of occurrence of cross-over of 95% and probability of mutation of 10%. Stopping criteria are defined based on a limited number of generations or by limiting the number of generations without improvement in the best fit. The structure of the GA is schematically shown in Fig. (7).

A. Design Variables

The design variables are organized in the vector $\bar{\mathbf{x}} = \begin{bmatrix}\mathbf{x}_{str} & \mathbf{x}_{sk} & \mathbf{x}_{geom}\end{bmatrix}$, concatenating the sets of geometry design variables $\mathbf{x}_{geom}$, stringer laminate $\mathbf{x}_{str}$ and skin laminate $\mathbf{x}_{sk}$. Geometric design variables are the stringer height h, stringer foot size b_{str} and unit cell width b, which ultimately determines the number of stringers in the full panel. Discrete values for geometry design variables were defined based on practical design guidelines employed in the design of aircraft stiffened panels [39]. Regarding stringer spacing, or the width of the panel unit cell, b, design variable discrete values corresponds to integer subdivisions of an entire wing bay panel of 840 mm wide.

There are two design variables required per ply in the stringer laminate: the orientation angle θ_i and its thickness t_i, in a similar approach shown in T-THETA method employed by Castro et al. [40]. The choice of number of plies is left to the optimizer to decide by specifying a vector to store a great amount of layers. The existence or absence of material in the i^{th} ply is controlled by the ply thickness: when $t_i = 1$ material is assigned and when $t_i = 10^{-5}$, the corresponding ply is disregarded while creating the finite element model. Fiber orientation angles for constant stiffness laminates can only assume 0, ±45 or 90^o. Skin design variables corresponds to the laminate stacking sequence using VSL formulation. A 3×3 uniform grid is used to map the skin surface of the panel unit cell, enabling the use of the Lagrangian polynomial-based interpolation, as per Eq. (2).

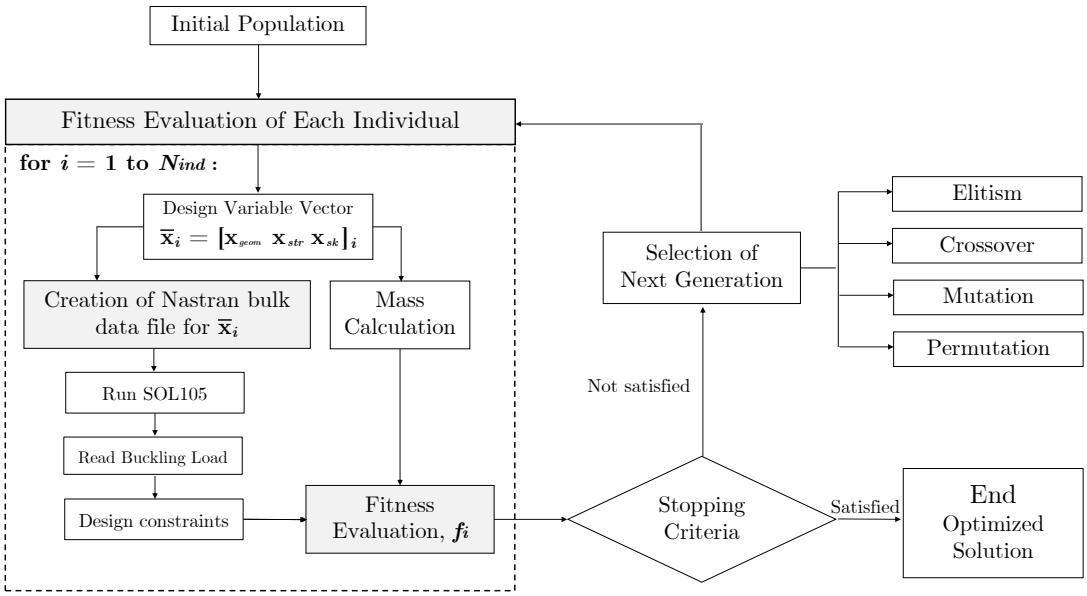

Fig. 7 Genetic Algorithm Scheme

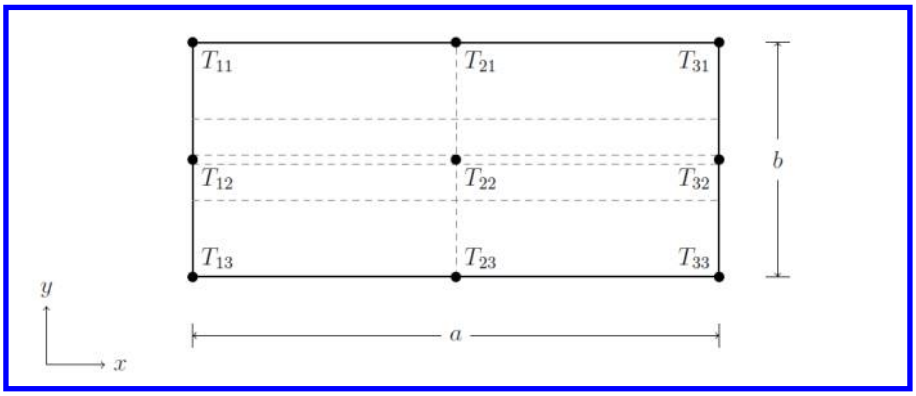

Fig. 8 Uniform 3×3 grid of reference points at the unit cell skin surface

Fiber continuity between two adjacent unit cells in the chord-wise direction is obtained assuming symmetry with respect to the longitudinal stiffener, located at $y = b/2$ and represented by the dashed lines in Fig. 8. Hence, the prescribed angles at $y = 0$ and $y = b$ should be the same, i.e., $T_{11} = T_{13}$, $T_{21} = T_{23}$ and $T_{31} = T_{33}$. For variations in both x and y-directions, symmetry with respect to the rib placed at $x = a/2$ can be imposed making $T_{11} = T_{31}$ and $T_{12} = T_{32}$, reducing the number of prescribed angles from nine to four. If angle variations are assumed only along the y-direction, then $T_{11} = T_{21}$ and $T_{12} = T_{22}$, reducing the problem to only two independent ply orientation angles. Each ply in the stacking sequence is fully described by the angles T_{mn} at the reference points and the thickness t_i, indicating which material is assigned to the i^{th} ply, in a similar manner that is performed in the stringer codification. For variations in one direction, the design variables per ply is represented by $x_{ski} = [T_{11}, T_{12}, t_i]$. The notation for variable stiffness layer in this work follows the notation introduced by Gürdal and Olmedo [3] as $\phi\langle T_{11}, T_{12}\rangle$, where ϕ is the angle with respect to the global coordinate system - assumed as zero in this work - reducing the notation simply to $\langle T_{11}, T_{12}\rangle$. Table 1 summarizes all the values that each discrete design variable can assume in the proposed optimization scheme. The design parameterization herein adopted leaves to the optimizer to decide on the number of plies for all laminates. Each laminate design variable vector is defined to be long enough to accommodate a maximum of 40 balanced plies, providing a wide design space to be explored. A ply is removed at a given position by the genetic algorithm if the

thickness value assigned to that ply is set to 10^{-5} in the denominated T-THETA approach [15].

Table 1 Summary of Optimization Design Variables

Design Variable		Values
$\mathbf{x}_{geom}$	b	105, 120, 140, 168, 210, 280 mm
	b_{str}	30, 40, 50, 60, 70 mm
	h	40, 50, 60, 70, 80, 90 mm
$\mathbf{x}_{str}$	θ	0, ±45, 90^o
	t_i	10^{-5}, 1
$\mathbf{x}_{str}$	T_{11}	0, 5, 10, 15, . . . , 60, 65, 70, 75 ^{o}
	T_{12}	
	t_i	10^{-5}, 1

B. Objective Function

The optimization problem in this study consists of:

- *(i)* Minimization of the mass m of a wing bay upper skin panel;
- *(ii)* Subjected to design constraints, $g_i(\bar{\mathbf{x}})$

Each individual fitness value is calculated as a function of the total mass of the panel, m, and the penalty factor functions associated with design constraints, $g_i(\bar{\mathbf{x}})$, according to Eq. (8):

$$f(\bar{\mathbf{x}}) = \left(\prod_{i=1}^{4} g_i(\bar{\mathbf{x}})\right) N_{stf}\ m_{unit}(\bar{\mathbf{x}}) \tag{8}$$

The mass of the unit cell, m_{unit}, is calculated in terms of design variables $\bar{\mathbf{x}}$, that contains information regarding geometry of the longitudinal stiffener and the number of layers in the skin, stringer and stringer foot laminates. The unit cell width b determines the number of longitudinal stiffeners N_{stf} within the full wing bay panel, so the total mass of the wing bay upper panel is obtained by the product $N_{stf}\ m_{unit}(\bar{\mathbf{x}})$. Each design constraint is associated to a penalty factor function g_i that assumes different values to increase f if not satisfied, being interpreted by the GA as a virtual increase in the total panel mass for unfit individuals. If all design constraints are satisfied, all penalty factor functions g_i are equal to one and the objective function becomes numerically equal to the panel mass.

There are four design constrains to be satisfied in the optimization framework. The first requires the critical buckling load P_{cr} obtained by MSC Nastran® to be higher the applied load P_a, hence the first eigenvalue shall respect $\lambda_1 \geq 1$ once λ_1 is defined as $\lambda_1 = P_{cr}/P_a$. Penalization for the eigenvalue constraint is applied according to Eq. (9), as proposed by the work of Groh and Weaver [35], as function of the first eigenvalue itself.

$$g_1(\lambda) = \max\left(1, \frac{1}{{\lambda_1}^2}\right) \tag{9}$$

Constraints regarding constant stiffness laminates are relative to ply percentage and ply contiguity. Design guidelines for the laminate composition requires a minimum percentage of plies in each orientation to be at least 10% of the laminate composition. In addition, the ply contiguity constraint limits the maximum number of consecutive plies with the same orientation that can be stacked together to 4, as plies with same orientation next to each other leads to matrix crack forming [37]. Violations in these two constraints are penalized by a factor of 1.5.

Regarding the manufacturing process of variable stiffness laminates (AFP or CTS), the manufacturing constraint is related to the minimum turning radius r_{min}, which is calculated for every VSL ply and shall be higher than the minimum allowed steering radius r_{allow} for the corresponding manufacturing process; in this work, the minimum allowed steering radius are 500 mm for AFP, 50 mm for CTS. Violations in these constraints are penalized by a factor of 3.0. Penalization factors were defined after a series of trial-and-error tests, focusing to not over-penalize unfit individuals so that genetic variability over generations are lost.

C. Loading

In early stages of an aircraft development, it is highly desirable to have a rapid tool that is capable of performing calculations with certain level of reliability so that decision making process is guided by solid engineering arguments. The complexity of the analysis method shall increase progressively as the design advances through the product development stages. Based on this design philosophy, this study relies on a rapid tool to calculate loads acting on a representative unit cell of the panel, considering a single load case due to a wing up-bending causing pure compression on the unit cell. This work uses a simple approach to estimate bending moments considering the wing as a cantilever beam subjected to the aircraft weight is distributed over the wing semi-span. The bending moment is determined by resolving the equilibrium equations for a cantilever beam, resulting in a design bending moment of approximately 215 kNm at the wing root, which is used as an input to all wing bay optimization process.

To determine direct stresses over a given section of the wing at a preliminary design phase, a structural idealization of the wing root cross-section is employed. In this structural idealization, longitudinal stiffeners are idealized as concentrated areas in such form that bending stresses are carried only by stringers whereas shear stresses are carried only by skin panels [41]. Bending stresses are determined by Eq. (10).

$$\sigma_x = \left(\frac{M_z I_{yy} - M_y I_{yz}}{I_{yy} I_{zz} - I_{yz}^2} \right) y + \left(\frac{M_y I_{zz} - M_z I_{yz}}{I_{yy} I_{zz} - I_{yz}^2} \right) z \tag{10}$$

This method becomes particularly interesting to the present study as the actual wing bay section needs to be discretized into booms to determine stress acting on the skin, based on certain parameters such as skin and stiffener thicknesses and geometries. In the optimization problem, the design variables within each individual evaluated in the genetic algorithm defines an unique skin-stringer assembly, with a given geometry and skin and stringer thicknesses that automatically determines the configuration of the booms but also determine the most stressed skin-stringer assembly within a wing bay.

The peak stress in the upper skin panel is used to define the compression state for the entire upper panel, by simply multiplying the acting stress by the skin-stringer assembly cross-sectional area. With this scheme approach, each individual stiffener, with the adjacent skin pockets, carries the correct design load with consistent compressive stresses generated thereof as a function of the optimization design variables.

VI. Verification of the Genetic Algorithm

To verify the proposed genetic algorithm and its overall robustness and convergence capabilities, the study preseted by Le Riche and Haftka [6] is used, where a laminate composite plate with 64 plies, simply supported at the four edges, is subjected to a bi-axial load as depicted in Fig. (9). The stacking sequence is optimized to maximize the buckling load factor. In this example, $a = 20$ in, $b = 10$ in, $N_x = N_y = 1$ lb. The laminate properties for the graphite-epoxy plate considered in this case, according to [6], are $E_1 = 18.5 \times 10^6$ psi, $E_2 = 1.89 \times 10^6$ psi, G =0.93×10^6 psi, $\nu_{12} = 0.3$, $t_{ply} = 0.005$ in, $\epsilon_1^{ua} = 0.008$, $\epsilon_2^{ua} = 0.029$, $\gamma_{12}^{ua} = 0.015$.

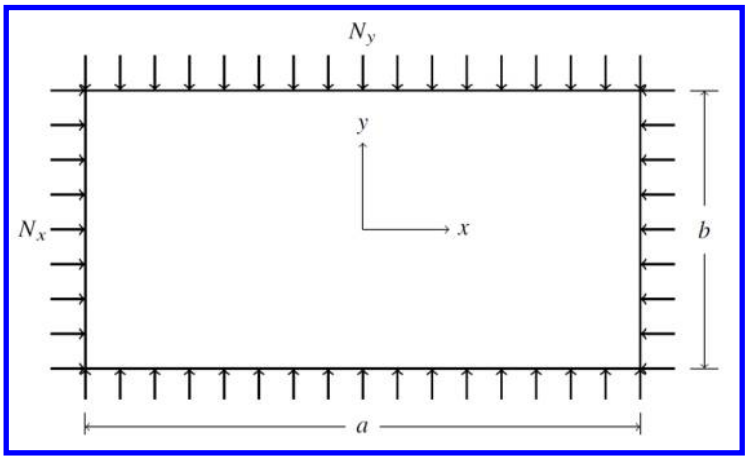

Fig. 9 Bi-axially loaded rectangular plate

The GA capability to search for the best solution is demonstrated as the same buckling load presented by the work of Le Riche and Haftka [6] has been found. Although the stacking sequence found by the GA is slightly different in terms of proportions of 90° or ±45° layers, it is noticeable that layup shares a lot of similarities with the five laminates presented in Table (2).

The optimization of panels involves more complex methods to evaluate the fitness function (e.g creation of Nastran bulk data files and running finite element analysis). Despite the different methods to evaluate each individual within a generation, the GA structure is exactly the same as used in the successful verification herein presented.

Table 2 Verification of the proposed genetic algorithm

Study	Stacking Sequence	Load Factor	
		Buckling	Failure
Le Riche and Haftka [6]	$[90_{10}, \pm 45_2, 90_2, \pm 45_3, 90_2, \pm 45_4]_S$	3973.01	14205.18
	$[\pm 45, 90_{10}, \pm 45, 90_8, \pm 45, 90_8]_S$	3973.01	8935.74
	$[90_4, \pm 45_2, 90_{16}, \pm 45, 90_6]_S$	3973.01	8935.74
	$[90_2, \pm 45, 90_6, \pm 45, 90_8, \pm 45, 90_{10}]_S$	3973.01	8935.74
	$[90_8, \pm 45, 90_2, \pm 45, 90_2, \pm 45, 90_2, \pm 45_6]_S$	3973.01	14205.18
Proposed GA	$[90_5, \pm 45, 90_4, \pm 45, 90_3, \pm 45, 90_5, \pm 45_2, 90_3, \pm 45]_S$	3973.01	11619.78

VII. Results

Four independent studies were performed in the following scenarios: (*i*) first, the baseline design is optimized using constant stiffness, symmetric and balanced laminates in both skin and stringer; (*ii*) AFP considering the manufacturing process employing the cut-and-restart technique, which allows constant thickness plies by avoiding the formation of overlaps; (*iii*) AFP with variable thickness, where the thickness build-up is a consequence of overlapping tows; (*iv*) CTS, where the steering-thickness coupling is inherent to the shearing process. For all variable stiffness cases, all variable stiffness layers are balanced to each other. The optimized design parameters for each stiffened panel are summarized in Table (3).

Table 3 Design parameters of the optimized panels

Parameter	Baseline	AFP, constant thickness	AFP, variable thickness	CTS
Width, b	105 mm	120 mm	120 mm	120 mm
Stringer Foot width, b_{st}	30 mm	50 mm	50 mm	40 mm
Stringer Height, h	40 mm	40 mm	40 mm	40 mm
Layers in stringer, N_{str}	30	32	34	32
Layers in stringer foot, N_{sf}	15	16	17	16
Layers in skin, N_{sk}	14	8	8	10
Minimum steering radius, r_s	-	502 mm	502 mm	55 mm
Applied load, F	116 kN	126 kN	132 kN	130 kN
Number of Unit Cells	8	7	7	7
Mass of Unit Cell	0.3063 kg	0.3027 kg	0.2457 kg	0.3000 kg
Mass of Panel	2.442 kg	2.119 kg	2.079 kg	2.100 kg
Weight Reduction	-	-13%	-15%	-14%

Note that the three variable stiffness panels have comparable weight, and achieved a weight reduction of $13-15\%$ compared to the baseline design. Although there is no significant weight differences among the different variable stiffness designs, they are considerably different among each other. The baseline panel, based on straight-fiber laminates, used the maximum number of stiffeners towards the optimal individual, represented by the minimum width b allowed,

Table 4 Stacking Sequence of Optimized Stiffened Panels

Optimization Case	Part	Stacking Sequence
Baseline	Stringer	$[\pm 45, 0, 90, 0, \pm 45, 0_2, \pm 45, 90, 0_2, 90]_S$
	Skin	$[\pm 45, 90, \pm 45, 90, 0]_S$
AFP, constant thickness	Stringer	$[\pm 45, 90_2 \pm 45, 0_2, 90, \pm 45, 0_2 \pm 45, 0]_S$
	Skin	$[\pm\langle 70, 60\rangle, \pm\langle 70, 65\rangle, \pm\langle 75, 65\rangle, \pm\langle 70, 75\rangle]$
AFP, variable thickness	Stringer	$[\pm 45_2, 0_2, 90, 0_2, 90, 0_3, \pm 45, 90, 0]_S$
	Skin	$[\pm\langle 60, 60\rangle, \pm\langle 70, 60\rangle, \pm\langle 70, 75\rangle, \pm\langle 60, 60\rangle]$
CTS	Stringer	$[0_2, \pm 45, \pm 45, 90, 0, 90, 0, \pm 45, \pm 45]_S$
	Skin	$[\pm\langle 75, 35\rangle, \pm\langle 55, 60\rangle, \pm\langle 65, 10\rangle, \pm\langle 55, 50\rangle, \pm\langle 70, 25\rangle]$

with the smallest stiffener's cross section. For the two AFP and the CTS designs, the minimum steering angle was reached at the corresponding optima, meaning that the maximum steering potential was explored by the optimizer. The CTS design has the same number of stiffeners as the AFP designs, with a slightly lower cross-sectional area, compensated by the larger thickness build-up on the skin.

A fitness-based convergence criteria is employed in the proposed GA, taking into account the evolution in the fitness value of the best-fit individual over the course of generations. The GA automatically sets a minimum of 100 generations to be run, and convergence is achieved within this boundary if there is no significant improvement in the best fitness value for the last 30 generations of the optimization; however, if convergence criteria is not achieved within the minimum 100 generations, the algorithm is capable of running more generations until the same fitness-based convergence criteria is properly achieved. The evolution of the fitness function, for all four cases studied, is shown in Fig. (10). The curve shows the evolution of the best fit individual within a generation throughout the optimization process.

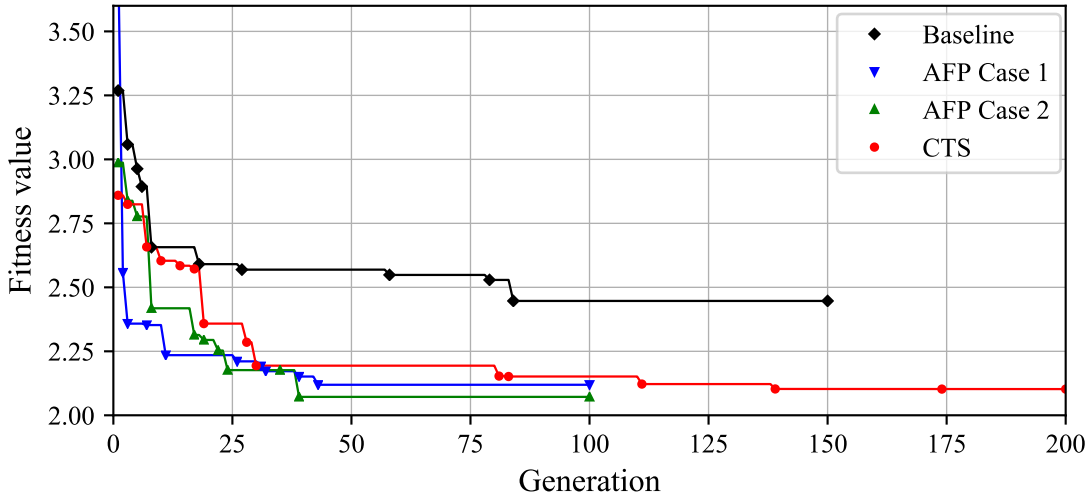

Fig. 10 Genetic Algorithm Optimization Convergence

The laminate stacking sequences obtained in the four optimized cases are shown in Table (4). For variable stiffness, each layer is shown according to the notation $\pm\langle T_{11}, T_{12}\rangle$, with the $\pm$ sign indicating that the layers are balanced in the present study.

Figures (11) and (12) show the layers with variable thickness obtained in the optimization of cases (*iii*) AFP with variable thickness and (*iv*) CTS, respectively. The thickness build-up in the AFP case is due to overlaps formed by the tow steering, as depicted in Fig. (11), where thicker overlapping regions are colored with darker shades. The CTS layers presented in Fig. (12) have a continuous thickness distribution over the plane due to the in-plane shear applied by this manufacturing method, where thicker regions are also represented by darker shades on the contour plot.

Exploded views of the layup obtained for the AFP with variable thickness and CTS cases are shown in Figs. (13) and (14), respectively. Only one ply of each balanced pair is included in the visualizations and layers with only straight fibers are omitted. The polar plots showing the membrane stiffness for the skin AFP design with variable thickness, in Fig. (13), shows that the skin is soft, in the sense that the stiffener is providing much of the axial load carrying capacity of the panel. On the other hand, for the CTS design the skin layers have fibers more aligned with the load in the region where the stiffener is located, as shown in Fig. (14). The polar plot for the CTS design at control point T_{12} clearly shows how the skin membrane stiffness is aligned with the load, and how the membrane stiffness changes rapidly from T_{11} to T_{12}. Such tailoring potential is due to the small minimum steering radius of the CTS process.

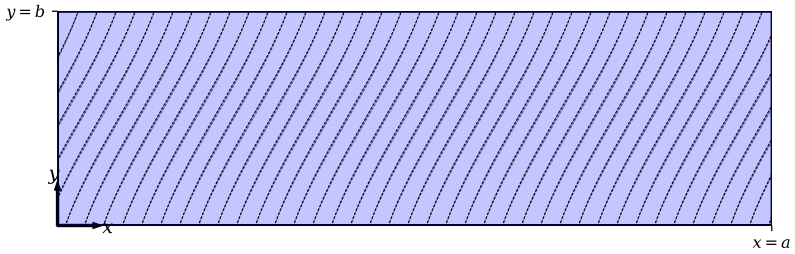

(a) $\langle 70, 60 \rangle$

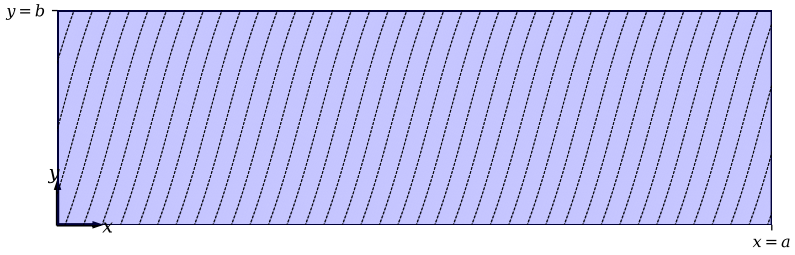

(b) $\langle 70, 75 \rangle$

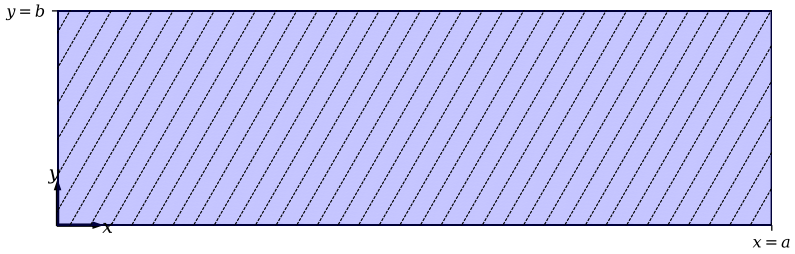

(c) $\langle 60, 60 \rangle$

Fig. 11 Variable stiffness layers for AFP with variable thickness. Straight-fiber layers are omitted. The tow widths are exaggerated for a better visualization.

In addition to Figs. (13) and (14), the membrane stiffness of all optimized configurations are shown in detail in Figs. (15) and (16) for stringer and skin, respectively. Comparing both AFP skin designs optimized in this study, the membrane stiffness distribution at the interpolation reference points is equivalent due to the similarity achieved by the GA in the parametrization of VSL layers for both AFP cases.

In terms of stringer membrane stiffness, the baseline plot shows how the longitudinal stiffener is responsible for providing the majority of axial load carrying capacity of the panel, as a result of the layup having more fibers aligned in the load direction, in a same pattern that is also presented in the AFP with variable thickness design.

In the present study, the load that is carried by each representative section is a function of the number of longitudinal stiffeners in the whole stiffened panel being analyzed, as well as the geometry of the representative section. The design load is divided among the subdivisions of the entire stiffened panel, meaning that increasing the number of longitudinal stiffeners favours optimal designs based on a linear buckling criteria. For all cases tested, the optimal designs found are those where the geometry design variable b assumed values of 120 mm or 105 mm (corresponding to 7 and 8

longitudinal stiffeners, respectively). From a design standpoint, this result is quite reasonable as it is highly desirable to decrease stringer spacing to increase buckling resistance of stiffened panels. The stringer height h was taken to the minimum value allowed in all cases, because local buckling of the stiffener's flange is an active constraint on all the design optima herein presented. Future studies should investigate the use of other stiffening profiles less subject to flange buckling.

The steering radius plays a major role in the resultant design, specially when comparing the two different manufacturing processes. Due to the constraining steering radius of 500 mm for AFP, smaller angle variations between the Lagrangian reference points placed at the center and the edge of the unit cell are observed, not exceeding more than 10^{o} for all AFP cases. In the other hand, the CTS case constraining steering radius corresponds to a tenth of the former, hence the feasible region in the design space allows more curved paths with higher angle variations between reference points.

Smaller angle variations between reference points also result in smaller overlaps between adjacent tows, as observed in the AFP case with coupled variable thickness. Comparing the two AFP cases optimized in this work, there is no significant differences in weight achieved by the optimization of the constant and variable thickness designs. However, the manufacturing of a constant thickness variable stiffness laminate requires the cut–and-restart to prevent overlaps, with the drawback of having a significantly higher manufacturing time.

Regarding the variable thickness of the laminates, the retrieved layups for each case show that, for both AFP and CTS designs, the overall local thickening is observed at the center of the unit cell, where the longitudinal stiffener is located. Physically, this means a thicker and stiffer region near the stiffener's foot, allowing a reduced stiffener to be used, as shown by the smaller optimum value for the stiffener's height in the CTS design.

VIII. Conclusion and Future Work

This work presented design concepts, parameterization schemes and the optimization of axially loaded stiffened panels, considering variable stiffness laminates for the panel skin with coupled steering-thickness. A genetic algorithm developed in Python programming language was used as the optimizer. The finite element method was used to perform buckling analyses, with MSC Nastran. The proposed design parameterization considered the panel geometry and laminate layups of the skin and stiffener as design variables.

Three different designs were optimized: AFP with constant thickness; AFP with coupled steering-thickness; and CTS with coupled steering-thickness. For each case, the inherent manufacturing constraints were considered. A baseline design based on straight fibers was used for comparisons. The three designs based on variable stiffness laminates showed a weight saving in the range of $13 - 15\%$, comparing the mass for one bay of the wingbox.

A smaller representation of the wing bay panel is achieved by means of a unit cell, thus reducing the required number of design variables to describe the entire wing bay panel. In this approach, the full panel can be reconstructed by using repeatedly the optimized representative unit cell. The conservatism in this method is that the unit cell is optimized based on most stressed stringer-skin assembly within the panel. By using this modular design approach, all other stringer-skin assembly within the panel are subjected lower stresses. Future studies should explore further weight savings by optimizing each stringer-skin assembly according to their respective load. Moreover, all wing bays could be optimized individually and the weight of the whole wing upper panel used in the fitness function.

The optimization performed in this work only focused on the buckling of axially loaded stiffened panels, not considering multiple load cases and the laminate strength. Future work shall include other structural failure modes in addition to buckling in the optimization framework. The use of genetic algorithms provided a robust optimization scheme even for the steering-thickness coupling considered in the AFP design with variable thickness and in the CTS design. However, the GA optimization requires thousands of individual evaluations, and future studies should look into means of performing an optimization based on stiffness parameters such as lamination parameters and the total thickness; however, with the total thickness depending on the final steering angle.

Acknowledgements

The authors acknowledge the support of EMBRAER and FCMF - Fundação Casimiro Montenegro Filho by the scholarship granted to the first author.

References

[1] Kim, B. C., Potter, K., and Weaver, P. M., "Continuous tow shearing for manufacturing variable angle tow composites," *Composites Part A: Applied Science and Manufacturing*, Vol. 43, No. 8, 2012, pp. 1347–1356.

[2] Blom, A. W., "Structural Performance of Fiber-Placed, Variable-Stiffness Composite Conical and Cylindrical Shells," Phd in aerospace engineering, Delft University of Technology, 2010.

[3] Gürdal, Z., and Olmedo, R., "In-plane response of laminates with spatially varying fiber orientations-variable stiffness concept," *AIAA journal*, Vol. 31, No. 4, 1993, pp. 751–758.

[4] Castro, S. G. P., Donadon, M. V., and Guimarães, T. A. M., "ES-PIM applied to Buckling of Variable Angle Tow Laminates," *Composite Structures*, Vol. 209, 2018, pp. 67–78.

[5] Kim, C., and Lee, J., "Optimal Design of Laminated Composite Plates For Maximum Buckling Load Using Genetic Algorithm," *Proceedings of The Institution of Mechanical Engineers Part C-journal of Mechanical Engineering Science - PROC INST MECH ENG C-J MECH E*, Vol. 219, 2005, pp. 869–878. https://doi.org/10.1243/095440605X31751.

[6] Le Riche, R., and Haftka, R. T., "Optimization of Laminate Stacking Sequence for Buckling Load Maximization by Genetic Algorithm," *AIAA Journal*, Vol. 31, No. 5, 1993, pp. 951–956.

[7] Nagendra, S., Jestin, D., Gürdal, Z., Haftka, R. T., and Watson, L. T., "Improved Genetic Algorithm for the Design of Stiffened Composite Panels," *Computers & Structures*, Vol. 58, No. 3, 1996, pp. 543–555.

[8] McIlhagga, M., Husbands, P., and Ives, R., "A comparison of search techniques on a wing-box optimisation problem," *Lecture Notes in Computer Science (including subseries Lecture Notes in Artificial Intelligence and Lecture Notes in Bioinformatics)*, Vol. 1141, Springer Verlag, 1996, pp. 614–623. https://doi.org/10.1007/3-540-61723-X_1025, URL https://link.springer.com/chapter/10.1007/3-540-61723-X_1025.

[9] Wan, Z., Yang, C., and Li, Z., "Application of hybrid genetic algorithm in aeroelastic multidisciplinary optimization," *Beijing Hangkong Hangtian Daxue Xuebao/Journal of Beijing University of Aeronautics and Astronautics*, 2004.

[10] Arizono, H., and Isogai, K., "Application of genetic algorithm for aeroelastic tailoring of a cranked-arrow wing," *Journal of Aircraft*, 2005. https://doi.org/10.2514/1.392.

[11] Gasbarri, P., Chiwiacowsky, L. D., and De Campos Velho, H. F., "A hybrid multilevel approach for aeroelastic optimization of composite wing-box," *Structural and Multidisciplinary Optimization*, Vol. 39, No. 6, 2009, pp. 607–624. https://doi.org/10.1007/s00158-009-0429-6, URL https://link.springer.com/article/10.1007/s00158-009-0429-6.

[12] Castro, S. G., Hernandes, J. A., and Lucena Neto, E., "Composite wing optimization with progressive mesh refinement," *20th International Congress of Mechanical Engineering*, Gramado, RS, Brazil, 2009. URL https://www.researchgate.net/publication/233406731_Composite_wing_optimization_with_proggressive_mesh_refinement.

[13] Castro, S. G., Hernandes, J. A., Bussamra, F. L. d. S., and Ponciano, W. M., "Finding optimal genetic algorithm parameters for a composite wing optimization," *11th Pan-American Congress of Applied Mechanics (PACAM)*, Foz do Iguaçu, PR, Brazil, 2010. URL https://www.researchgate.net/publication/233406886_Finding_optimal_genetic_algorithm_parameters_for_a_composite_wing_optimization.

[14] Castro, S. G., Guimarães, T. A., and Hernandes, J. A., "Composite optimization performance comparison between GENESIS (R) BIGDOT and ModeFrontier (R) MOGAII algorithms," *VI NATIONAL CONGRESS OF MECHANICAL ENGINEERING (CONEM)*, Campina Grande – Paraíba – Brazil, 2010. URL https://www.researchgate.net/publication/233406745_Composite_optimization_performance_comparison_between_GENESIS_R_BIGDOT_and_ModeFrontier_R_MOGAII_algorithms.

[15] Castro, S. G., Guimarães, T. A., and Hernandes, J. A., "Comparison of free stacking sequence approach versus a predefined 0/+45/-45/90 sequence in a typical aircraft wing optimization," *2nd International Conference on Engineering Optimization (ENGOPT)*, Lisbon, Portugal, 2010. URL https://www.researchgate.net/publication/233406751_Comparison_of_free_stacking_sequence_approach_versus_a_predefined_045-4590_sequence_in_a_typical_aircraft_wing_optimization.

[16] Jin, P., Song, B., and Zhong, X., "Structure optimization of large composite wing box with parallel genetic algorithm," *Journal of Aircraft*, Vol. 48, No. 6, 2011, pp. 2145–2148. https://doi.org/10.2514/1.C031493, URL https://arc.aiaa.org/doi/abs/10.2514/1.C031493.

[17] Liguori, F. S., Zucco, G., Madeo, A., Magisano, D., Leonetti, L., Garcea, G., and Weaver, P. M., "Postbuckling optimisation of a variable angle tow composite wingbox using a multi-modal Koiter approach," *Thin-Walled Structures*, Vol. 138, 2019, pp. 183–198. https://doi.org/10.1016/j.tws.2019.01.035.

[18] Wu, Z., Weaver, P. M., Raju, G., and Kim, B. C., "Buckling Analysis and Optimisation of Variable Angle Tow Composite Plates," *Thin-walled structures*, Vol. 60, 2012, pp. 163–172.

[19] van Campen, J., Kassapoglou, C., and Gürdal, Z., "Design of Fiber-steered Variable-stiffness Laminates Based on a Given Lamination Parameters Distribution," *Collection of Technical Papers - AIAA/ASME/ASCE/AHS/ASC Structures, Structural Dynamics and Materials Conference*, 2011. https://doi.org/10.2514/6.2011-1894.

[20] IJsselmuiden, S. T., "Optimal Design of Variable Stiffness Composite Structures using Lamination Parameters," Phd in aerospace engineering, Delft University of Technology, 2011.

[21] Sodja, J., Werter, N., and De Breuker, R., "Design of a flying demonstrator wing for manoeuvre load alleviation with cruise shape constraint," *2018 AIAA/ASCE/AHS/ASC Structures, Structural Dynamics, and Materials Conference*, American Institute of Aeronautics and Astronautics, Reston, Virginia, 2018. https://doi.org/10.2514/6.2018-2153, URL https://arc.aiaa.org/doi/10.2514/6.2018-2153.

[22] Vertonghen, L., and Castro, S. G. P., "Modelling of fibre steered plates with coupled thickness variation from overlapping continuous tows," 2020. https://doi.org/10.31224/OSF.IO/9BJY6, URL https://engrxiv.org/9bjy6/.

[23] Bisagni, C., and Vescovini, R., "Fast tool for buckling analysis and optimization of stiffened panels," *Journal of Aircraft*, Vol. 46, No. 6, 2009, pp. 2041–2053. https://doi.org/10.2514/1.43396, URL http://arc.aiaa.org.

[24] Vescovini, R., and Bisagni, C., "Buckling analysis and optimization of stiffened composite flat and curved panels," *AIAA Journal*, Vol. 50, No. 4, 2012, pp. 904–915. https://doi.org/10.2514/1.J051356, URL http://arc.aiaa.org.

[25] Vescovini, R., and Bisagni, C., "Semi-analytical buckling analysis of omega stiffened panels under multi-axial loads," *Composite Structures*, Vol. 120, 2015, pp. 285–299. https://doi.org/10.1016/j.compstruct.2014.10.003, URL https://linkinghub.elsevier.com/retrieve/pii/S0263822314005212.

[26] Castro, S. G., and Donadon, M. V., "Assembly of semi-analytical models to address linear buckling and vibration of stiffened composite panels with debonding defect," *Composite Structures*, Vol. 160, 2017, pp. 232–247. https://doi.org/10.1016/j.compstruct.2016.10.026, URL http://linkinghub.elsevier.com/retrieve/pii/S026382231631008Xhttps://linkinghub.elsevier.com/retrieve/pii/S026382231631008X.

[27] Castro, S. G., Guimarães, T. A., Rade, D. A., and Donadon, M. V., "Flutter of stiffened composite panels considering the stiffener's base as a structural element," *Composite Structures*, Vol. 140, 2016, pp. 36–43. https://doi.org/10.1016/j.compstruct.2015.12.056, URL https://doi.org/10.1016/j.compstruct.2015.12.056https://linkinghub.elsevier.com/retrieve/pii/S0263822315011460http://www.scopus.com/inward/record.url?eid=2-s2.0-84953212729&partnerID=MN8TOARS.

[28] Tatting, B. F., Gürdal, Z., and Jegley, D., "Design and Manufacture of Elastically Tailored Tow Placed Plates," *NASA/CR 2002-211919*, 2002, pp. 1–14.

[29] Gürdal, Z., Tatting, B. F., and Wu, C., "Variable stiffness composite panels: effects of stiffness variation on the in-plane and buckling response," *Composites Part A: Applied Science and Manufacturing*, Vol. 39, No. 5, 2008, pp. 911–922.

[30] de Quadros, H. B., and Hernandes, J. A., "A lagrange parametrization for the design of variable stiffness laminates," *Structural and Multidisciplinary Optimization*, Vol. 58, No. 1, 2018, pp. 129–137. https://doi.org/10.1007/s00158-017-1882-2, URL https://doi.org/10.1007/s00158-017-1882-2.

[31] Capacia, V. N., "Wing panel optimization using lamination parameters and inverse distance weighting interpolation." Ph.D. thesis, Dissertation of Master of Science – Instituto Tecnológico de Aeronáutica, São José dos Campos., 2018.

[32] Capacia, V. N., Castro, S. G. P., and Hernandes, J. A., "Composite Panel Optimization using Lamination Parameters and Inverse Distance Weighting Interpolation," *Proceedings of the International Congress of Mechanical Engineering (COBEM)*, Uberlândia, 2019. https://doi.org/10.26678/ABCM.COBEM2019.COB2019-1745.

[33] Clancy, G., Peeters, D., Oliveri, V., Jones, D., O'Higgins, R. M., and Weaver, P. M., "A study of the influence of processing parameters on steering of carbon Fibre/PEEK tapes using laser-assisted tape placement," *Composites Part B: Engineering*, Vol. 163, 2019, pp. 243–251. https://doi.org/10.1016/j.compositesb.2018.11.033, URL https://linkinghub.elsevier.com/retrieve/pii/S135983681832300X.

[34] Vertonghen, L., "Semi-Analytical Buckling and Optimisation of Variable Stiffness, Variable Thickness Laminates," Master of science in aerospace engineering, Delft University of Technology, 2019.

[35] Groh, R. M., and Weaver, P., "Mass Optimisation of Variable Angle Tow, Variable Thickness Panels with Static Failure and Buckling Constraints," *56th AIAA/ASCE/AHS/ASC Structures, Structural Dynamics, and Materials Conference*, 2015. https://doi.org/10.2514/6.2015-0452.

[36] Fenner, P., "Comparing the Accuracy of VICONOPT to FEM for Analysing Aircraft Wing Skin Type Panels," Master of science in aerospace engineering, Loughborough University, 2014.

[37] Kassapoglou, C., *Design and Analysis of Composite Structures: With Applications to Aerospace Structures*, New York, USA, 2013.

[38] MSC, *MSC Nastran Quick Reference Guide*, MSC Software, 2017.

[39] Niu, C., *Airframe Structural Design: Practical Design Information and Data on Aircraft Structures*, Conmilit Press LTD., 1988.

[40] Castro, S. G. P., Guimarães, T. A., and Hernandes, J. A., "Comparison of Free Stacking Sequence Approach (T-THETA) versus a Predefined 0/+45/-45/90 Sequence in a Typical Aircraft Wing Optimization," *Proceedings of the 2nd International Conference on Engineering Optimization (ENGOPT)*, Lisbon, 2010.

[41] Megson, T. H. G., *Aircraft Structures for Engineering Students*, 4th ed., Butterworth-Heinemann, 2007.

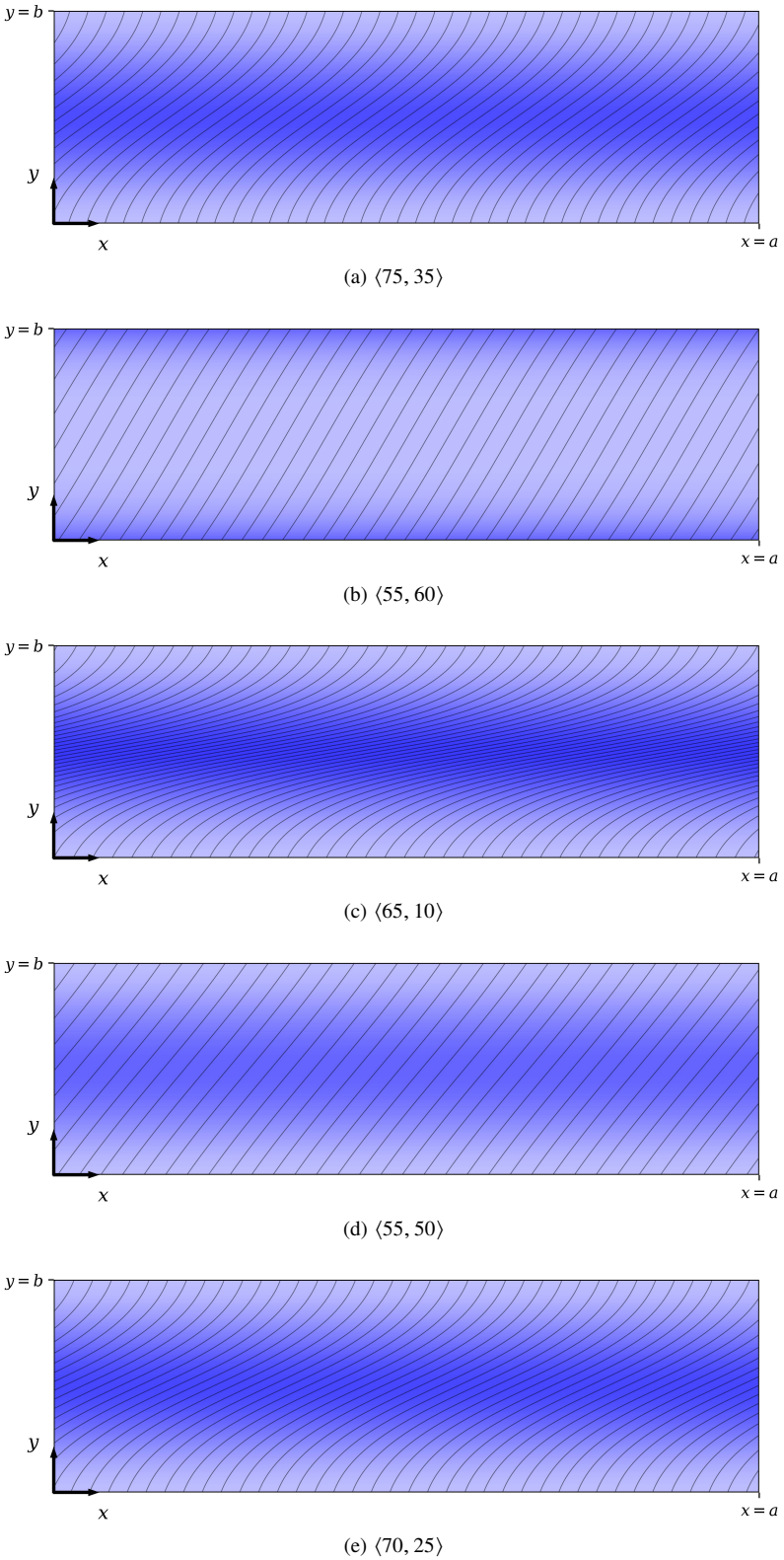

(a) ⟨75, 35⟩

(b) ⟨55, 60⟩

(c) ⟨65, 10⟩

(d) ⟨55, 50⟩

(e) ⟨70, 25⟩

Fig. 12 Variable stiffness layers for CTS. From (a) to (e), each layer represents one layer of the balanced pair according to the stacking sequence of Table (4)

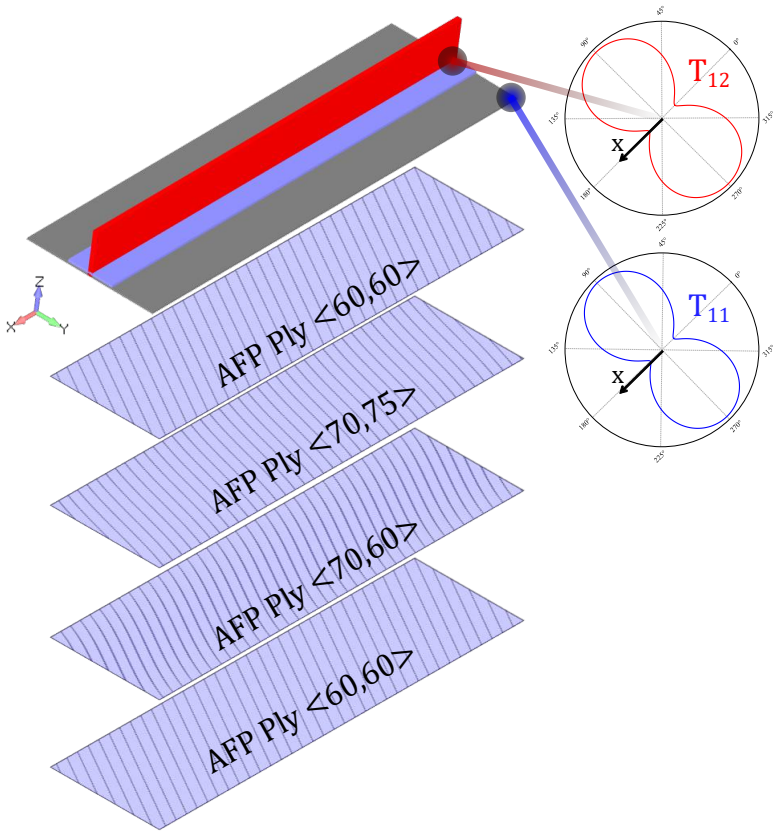

Fig. 13 Optimized skin design for AFP with variable thickness. The polar plots show the membrane stiffness in all directions for control points T_{11} and T_{12}.

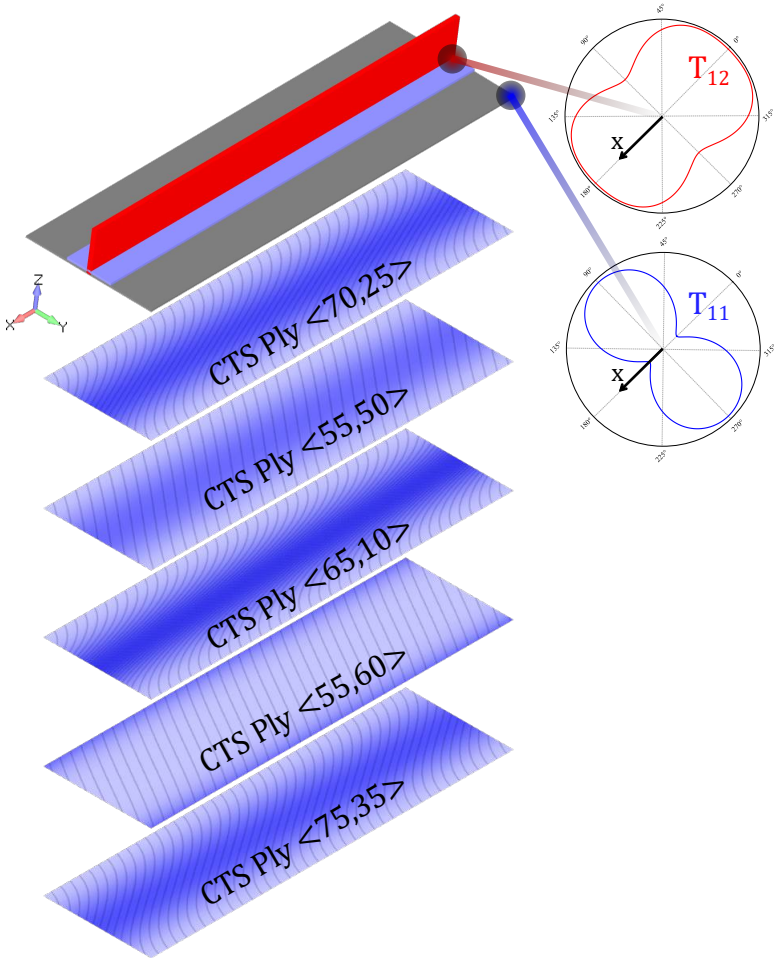

Fig. 14 Optimized skin design for CTS. The polar plots show the membrane stiffness in all directions for control points T_{11} and T_{12}.

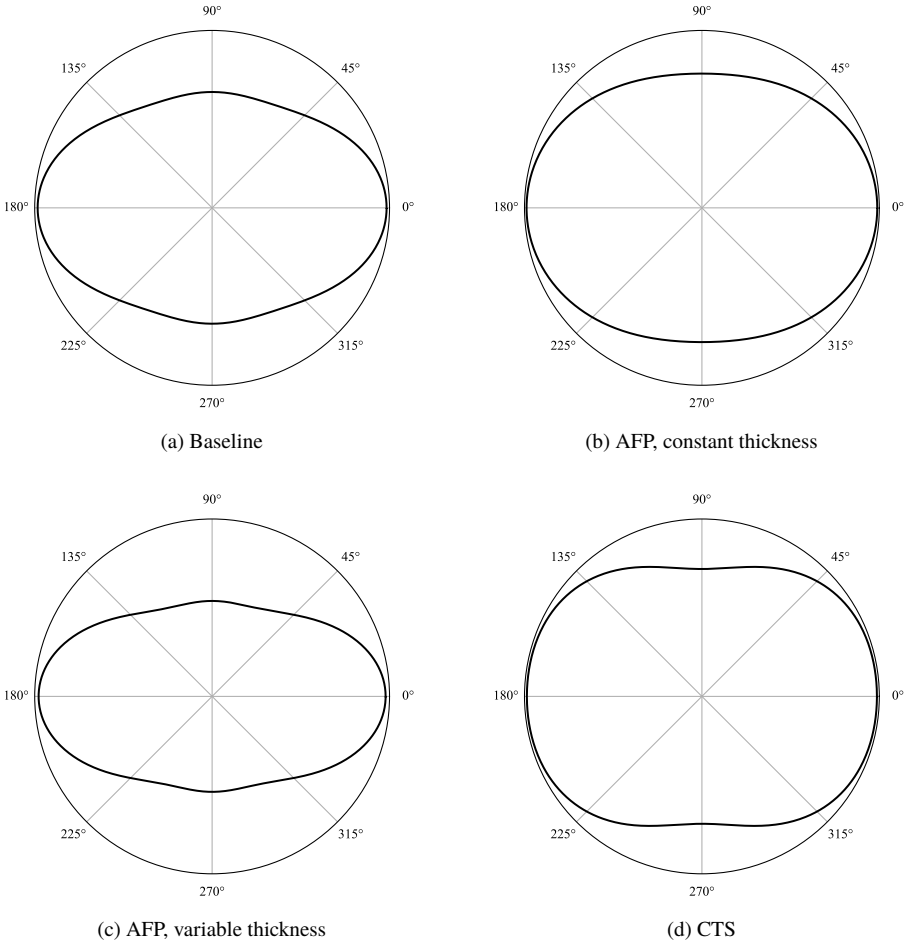

(a) Baseline

(b) AFP, constant thickness

(c) AFP, variable thickness

(d) CTS

Fig. 15 Stringer laminate polar plot

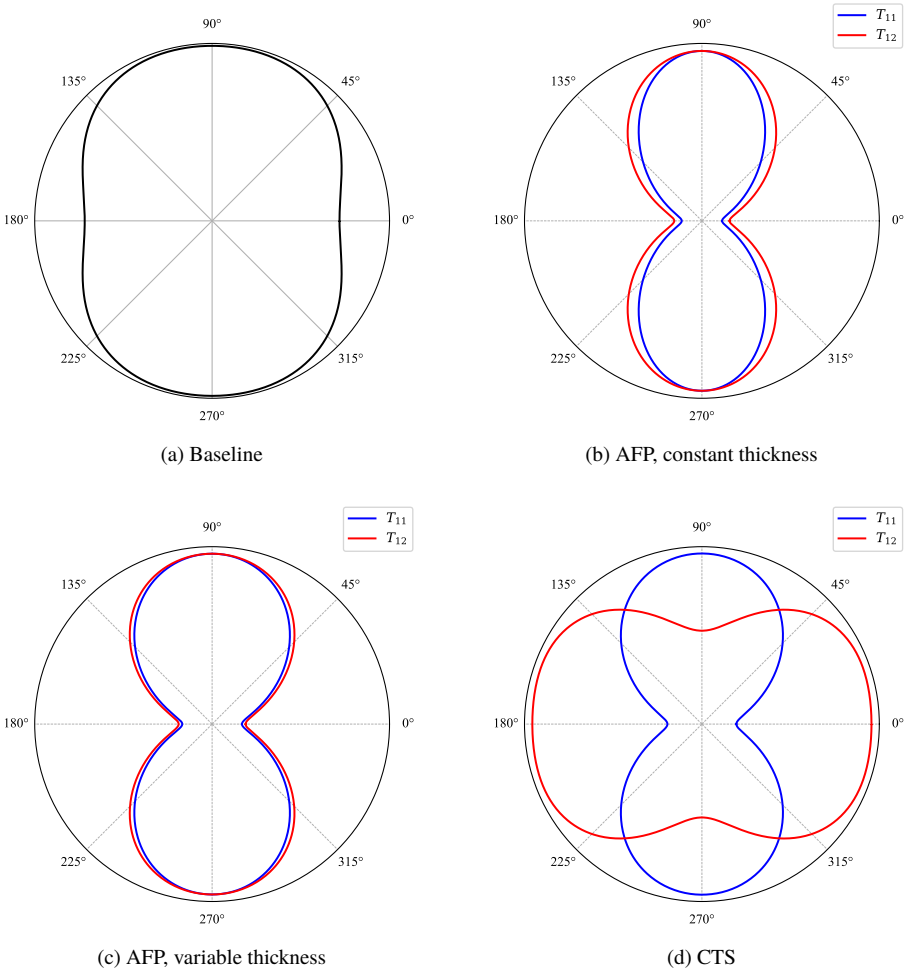

(a) Baseline

(b) AFP, constant thickness

(c) AFP, variable thickness

(d) CTS

Fig. 16 Skin laminate polar plot